Damage to Rock: Near Field Seismic Models Revisited

Santiago Gómez, José A. Sanchidrián, Pablo Segarra
Universidad Politécnica de Madrid – E.T.S.I. Minas y Energía

Abstract

This study points out the differences between two variants of the industry-standard Holmberg-Persson (H-P) calculation of vibrations from a blasthole in the near-field, and a semi-analytical vibration prediction model called full-field solution (FFS). The models have been calibrated through experimental data, which were obtained from two blasting campaigns. The seismic records were obtained by vertically oriented high-range accelerometers placed at radial distances between 2.7 to 28.3 m (2.9 to 30.9 yd) from the blastholes. The site specific constants of the H-P models have been estimated using peak velocities calculated by the FFS itself and the common simplification $\beta = 2\alpha$; this provides a best-case scenario for the comparison between models. The analysis is conducted at two levels: vibrations and rock damage. In the first one, we compare the peak particle velocity (*ppv*) radiation patterns, whereas in the second one we consider the extension of fracture zones for each model. The main difference between H-P and FFS is the directionality of the radiation patterns. This is attributable to the absence of shear waves and the infinite detonation velocity in the H-P approaches, causing ellipsoidal and nearly spherical radiation patterns that are not physically sound. This makes up different damage patterns, in which a smaller or non-existent crushed zone and a larger tensile cracked zone is observed in the H-P models with respect the FFS.

Introduction

Blast-induced rock damage is an important issue in underground and surface mining, and in tunnelling. It must be predicted in order to optimize drilling and blasting so that over-excavation, rock fall and slope failures would be limited, thereby improving the operation from the economic and safety angles. There is a variety of methods available to predict the extension of damaged zones due to blasting. Most commonly, they use vibration models based upon simple charge weight and distance scaling laws, to compute peak particle velocities (*ppv*) that, in combination with simple plane stress formulae, allow calculating the maximum stress in the rock at a given distance (Persson et al., 1993). The well-known Holmberg and Persson (H-P) approach (Holmberg and Persson, 1978) and related work by the National Institute for Occupational Safety and Health (NIOSH) (Hustrulid and Lu, 2003) (Iverson et al., 2008) provide simple engineering solutions most often applied to contour and buffer blastholes. Despite their physical flaws and limitations —Blair and Minchinton early criticised the use of vibration prediction models based on charge weight scaling laws in the 90s because of some invalid assumptions (Blair, 1990) (Blair and Minchinton, 1997)— they have been the preferred ones by most field engineers in the last forty years, and even today they are used in first line publications (see e.g. (Silva et al., 2019) (Salum and Murthy, 2019) (Gou et al., 2020)).

The basic analytical theory (Tubman, 1984) (Tubman et al, 1984) (Meredith, 1990) (Meredith et al., 1993), and the developments made by Blair (Blair, 2007) (Blair, 2010) (Blair, 2014), are taken as baseline for what Blair called full-field solution (FFS) (Blair, 2007). The term FFS stands for an exact solution in both the near-field and the far-field. The full-field solution (FFS) is seldom used by practitioners. However, its potential is unique for predicting vibrations, especially in the near-field. It considers the case of a pressurized equivalent dry cavity (Sharpe, 1942), with a load applied on the wall to model the blasthole. Analytic functions are available to represent the pressure-time history on the wall (Sharpe, 1942) (Duvall, 1953) (Ricker, 1953) (Blair and Minchinton, 1997) (Uenishi and Rossmanith, 1998) (Vanbrabant et al., 2002) (Blair, 2003) (Rossmanith and Kouzniak, 2004) (Cho and Kaneko, 2004) (Blair, 2007) (Blair, 2010) (Blair, 2015a) (Ahn and Park, 2017); however, although these functions are a simple way of representing the explosive action, they do not often model adequately the behaviour of the explosive due to large rise times or unrealistic pressure decay patterns (Blair, 2010).

Normally, the pressure applied at the explosive/rock interface is considered to peak at the von Neumann pressure (P_{VN}) (Blair, 2003) (Blair, 2007) (Blair, 2010) (Blair, 2014) (Blair, 2015b). This state is reached when a shock wave compresses the explosive along its unreacted hugoniot (Minchinton, 2015), i.e. it is a state of the unreacted explosive and not of the rock shock space. In this work the calculation of the peak pressure at the blasthole wall is based on an explosive-to-rock shock matching scheme that ensures a pressure consistent with the shock properties of the rock.

Outside the blasthole, the FFS considers the rock to be purely elastic (Blair, 2010). Attenuation may be introduced by means of simple constitutive models, which exhibit the ability to both store and dissipate strain energy (Meza-Fajardo and Lai, 2007), with propagation velocities being complex functions of frequency. The constant-Q (CQ) attenuation model in frequency (Kjartansson, 1979) is used for simplicity. This paper is a short version of a previous work (Gómez et al., 2020), in which the data, the mathematical foundations of the FFS and the comparison of radiation patterns from FFS and H-P approaches are described in detail.

Test site description and validation

A series of full-scale blasting tests were conducted at El Aljibe quarry in 2017 to 2019. The quarry is located near Almonacid de Toledo (Spain). It mines mylonite, a metamorphic, high strength rock mainly used for conventional and high-speed railway ballast. The blasts were located in the Southwest part of the lower level of the pit, out of the normal production zone of the quarry. The rock structure can be described as blocky. The mechanical properties of the rock were determined from five samples collected near the working area. They are shown in Table 1.

Table 1. Mechanical properties of the rock mass[1].

V_p (km/s/ft/s)	V_s (km/s/ft/s)	ρ (g/cm^3)	ν	E (GPa/ksi)	UCS (MPa/ksi)	TS (MPa/ksi)
5.84/19173.2	3.30/10841.2	2.72	0.24	74.76/10843	171.21/24.83	18.21/2.64

[1]V_p and V_s: p- and s-wave velocities; ρ: density, ν: Poison's ratio; E: Young's modulus; UCS: uniaxial compressive strength; TS: tensile strength

Four blasts called B3, B6, B7 and B9 were instrumented, each one consisting of one row of seven blastholes, with a diameter of 89 mm (3½ in), inclined 15° to 20° from the vertical to make them parallel to the free face of the bench. The explosive used in the tests was an emulsion. It was bottom initiated with 400 g (0.88 lb) boosters and electronic detonators. The blasts were fired from blasthole BH#7 towards blasthole BH#1 using a delay of 23 ms between holes. Three uniaxial ceramic-shear accelerometers, A1(10000 g), A2 (5000 g), and A3 (500 g), were used (1 g = 32.17 ft/s^2). All the sensors were vertically oriented and placed in pairs at the bottom of a vertical 6 m borehole behind the blasts. They were fixed to an aluminium block screwed to another aluminum piece plugging the end of a rigid PVC tube of 63 mm (2.48 in); both the plug and the bottom part of the tube were grouted to the hole walls ensuring a firm attachment of the sensors to the rock mass, while allowing to recover the sensors. Seismic signals were fed to two conventional acquisition units using a sampling rate of 10 MHz. The units were triggered by an electronic cap fired simultaneously with the leading hole BH#7. Detonation velocity and density of the explosive were also measured in the tests. As example, Figure 1 shows a waveform recorded.

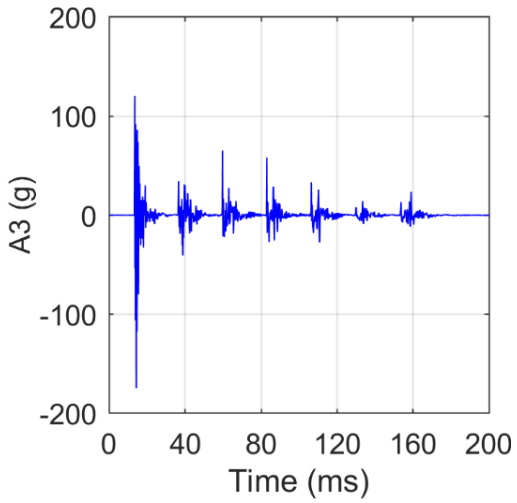

Figure 1. Waveform from A3 in blast B3.

Mathematical formulation

The H-P approach uses the basic equation of vibration propagation from a blasthole (Holmberg and Persson, 1978):

$$ppv = K \cdot W^{\alpha}/R^{\beta} \qquad \textbf{Equation 1}$$

where K, α and β are specific site constants, W is the total explosive charge and R is the distance. Dividing the explosive column into segments and adding the contribution of each element of explosive to the vibration at a point P (r_0, z_0) and setting $\beta = 2\alpha$, then Eq. (1) becomes:

$$ppv = Kq^{\alpha}\left\{\frac{1}{r_0}\tan^{-1}\left(\frac{z-z_0}{r_0}\right)\Big|_{z_i}^{z_f}\right\}^{\alpha} \qquad \textbf{Equation 2}$$

where zi and zf are the axial coordinates of the bottom and the top of the explosive charge, respectively.

The NIOSH-modified approach re-writes Eq. (1) as follows:

$$ppv = K \cdot W^{\alpha}/\bar{R}^{\beta} \qquad \textbf{Equation 3}$$

where $\overline{R}$ is the average distance to the observation point for all of the explosive elements; it can be calculated as:

$$\bar{R} = \frac{1}{C_L}\int_{z_i}^{z_f}\sqrt{r_0^2 + (z-z_0)^2}\,dz \qquad \textbf{Equation 4}$$

The FFS predicts the behaviour of the rock upon detonation of a cylindrical explosive charge. Any seismic field (displacement, velocity, etc.) may be represented based on three displacement potentials, one of them corresponding to a longitudinal or primary wave and the other two to transverse or shear waves (see e.g. Meredith 1990). To model the detonation, elements of small length transmit a load to the blasthole wall consecutively with a time difference equal to the travel time of the detonation front Blair (2010). The fundamental equation of the model is (refer to (Gómez et al., 2020) for deeper understanding of the parameters in the formula):

$$f_v = \frac{a^2}{2\pi^2}\int_{-\infty}^{\infty}\left\{\int_{-\infty}^{\infty}\left[\left(\sum_{\zeta=1}^{n}F_{\zeta}(r,k_z,\omega)\cos\gamma_{\zeta}\right)e^{ik_z z_1}\left(\frac{1-e^{i2LJ\left(-k_z+\frac{\omega}{D}\right)}}{1-e^{i2L\left(-k_z+\frac{\omega}{D}\right)}}\right)\right]dk_z\right\}e^{-i\omega t}d\omega \qquad \textbf{Equation 5}$$

where f_v is the vertical component of any field f at a certain location (r, z), ζ denotes the corresponding direction i.e., radial (r) or axial (z), a is the blasthole radius (m), F_{ζ} is the wavenumber-frequency transform of the ζ-component field. It depends on the radial distance to the monitoring point r, the axial wavenumber, k_z (rad/m), the angular frequency ω (rad/s) and the director cosines γ_{ζ} (see Figure 2); L is the half-length of an element of explosive (m), D is the detonation velocity (m/s), z_1 is the axial coordinate of the monitoring point as if it were seen from the center of the first element that detonates and t the time in seconds. Units must be consistent when using imperial system.

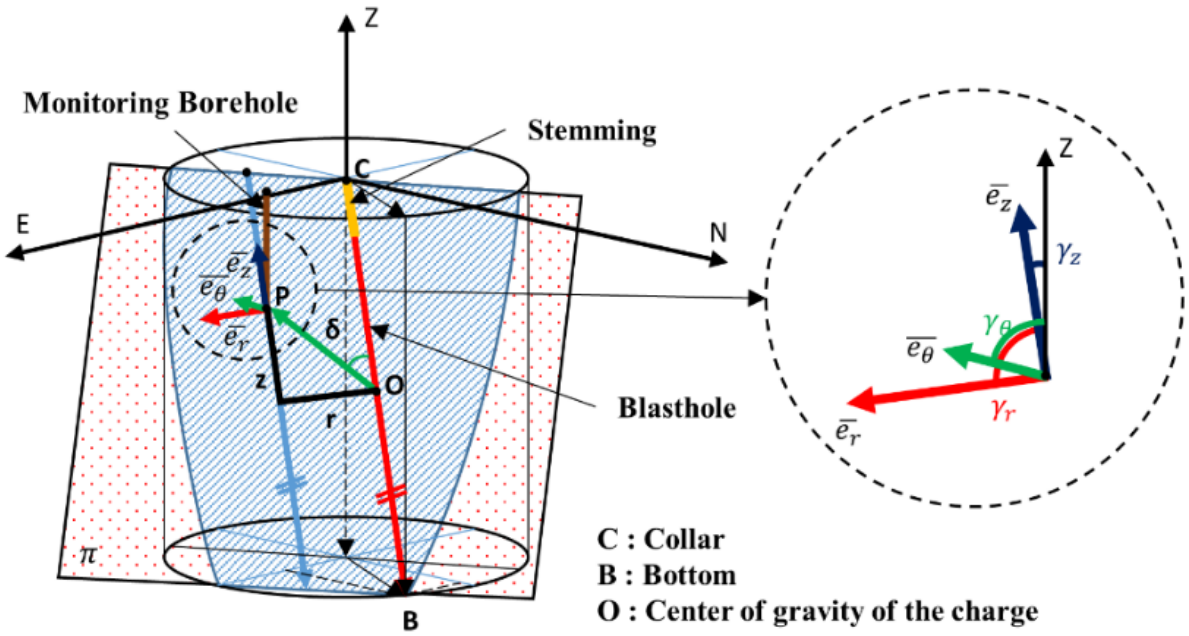

Figure 2. Sketch illustrating the calculations for an inclined blasthole.

F_ζ consists of three terms: the spectral response of the source function, a sinusoidal term, and a directional term (Blair 2010) (Gómez et al., 2020). The most important is the first one because vibration levels and frequency content depend largely on it. In this work, we use a pressure-time history obtained in the context of a wider project by numerically modelling the detonation. The directional term includes the attenuation model in the form of two-phase velocity functions dependent on angular frequency, one for each wave velocity. The problem is divided into two parts, one for each integral. The inner integral is solved numerically by using an adaptive quadrature method; the outer integral is solved using an Inverse Fast Fourier Transform algorithm. Local coordinates (r, z) and charge lengths, C_L, calculated using the scheme of Figure 2, are summarised in Tables 2 and 3, respectively.

Table 2. Local coordinates in m/yd.

BH	B3		B6		B7		B9			
	A2/A3		A2/A3		A2b/A3b		A1/G1		A2b/A3b	
	r	*z*	*r*	*z*	*r*	*z*	*r*	*z*	*r*	*z*
1	24.4/26.7	7.7/8.4	18.0/19.7	3.5/3.8	28.3/30.9	5.8/6.3	14.3/15.6	2.4/2.6	28.5/31.2	5.6/6.1
2	21.7/23.7	8.2/9.0	15.1/16.5	4.2/4.6	26.2/28.7	5.4/5.9	11.0/12.0	2.6/2.8	25.8/28.2	5.4/5.9
3	19.3/21.1	7.1/7.8	12.1/13.2	3.8/4.2	23.5/25.7	8.2/9.0	7.1/7.8	2.6/2.8	22.4/24.5	5.9/6.5
4	17.3/18.9	6.7/7.3	8.8/9.6	3.8/4.2	20.9/22.9	7.3/8.0	3.6/3.9	2.6/2.8	19.5/21.3	4.9/5.4
5	15.7/17.2	5.7/6.2	7.0/7.7	3.7/4.0	18.2/19.9	6.0/6.6	2.7/3.0	1.9/2.1	16.3/17.8	3.9/4.3
6	14.8/16.2	6.5/7.1	5.4/5.9	3.1/3.4	15.9/17.4	5.7/6.2	4.4/4.8	2.1/2.3	13.6/14.9	4.4/4.8
7	14.8/16.2	7.0/7.7	7.1/7.8	3.8/4.2	13.7/15.0	9.7/10.6	8.4/9.2	2.7/3.0	12.3/13.5	5.1/5.6

Table 3. Charge lengths in m/ft.

BH	B3	B6	B7	B9
1	11.9/39.0	11.6/38.0	11.1/36.4	11.7/38.4
2	10.6/34.8	11.4/37.4	10.3/33.8	12.0/39.4
3	11.0/36.1	11.1/36.4	12.4/40.7	12.4/40.7
4	11.2/36.8	10.9/35.8	12.9/42.3	12.8/42.0
5	10.7/35.1	10.9/35.8	11.9/39.0	11.0/36.1
6	11.6/38.0	11.1/36.4	12.2/40.0	12.6/41.3
7	11.9/39.0	11.4/37.4	2.7/8.9	12.8/42.0

Shock matching

The source function is scaled using the pressure at the explosive/rock interface (P_{SM}) that is determined by the intersection of the direct hugoniot of the rock with the reflected hugoniot of the detonation products at the Chapman-Jouguet (CJ)-point. This is based on the relationships governing the breakup of an arbitrary discontinuity resulting from the reflection of a shock wave from the contact surface between two media. See e.g. (Meyers, 1994) (Zel'dovich & Raizer, 2002). Details about the calculation of this peak pressure are shown in (Gómez et al., 2020). Explosive properties for each blast are summarized in Table 4.

Table 4. Explosive properties.

Blast	D (m·s^{-1}/ft·s^{-1})	ρ_e (g/cm^3)	P_{SM} (GPa/ksi)
3	4955.6/16258.5	1.154	9.39/1361.9
6	5306.0/17408.1	1.156	10.53/1527.2
7	5254.0/17237.5	1.152	10.34/1499.7
9	5956.4/19542.0	1.300	13.81/2003.0
Mean	5534.4/18152.8	1.193	11.54/1673.7

Calibration and validation

The seismic signals recorded are used to calibrate the model in amplitude by adjusting the Q-values of the constant-Q model (one for each wave type) so that the calculated peak accelerations fit the measured values. For this purpose, a code based on a root finding algorithm has been developed. The following procedure is followed: (i) Local coordinates (r, z), charge lengths, C_L, and director cosines, γ_ζ, are obtained for each blasthole from collar (C) and bottom (B) absolute coordinates and stemming lengths (see Figure 2 and Tables 2 and 3); (ii) arrival times are calculated using the propagation velocities of the rock mass in Table 1; (iii) experimental peak particle accelerations, *ppa*, associated with each propagation velocity are calculated using the arrival times in the recorded signals; (iv) a shock matching calculation is performed to calculate the peak pressure on the borehole wall; the explosive properties, the density and the shock-to-particle velocity linear relation constants of the rock are used; (v) Q-values are calculated for each blasthole location so that accelerations calculated match measured values and; (vi) two exponential Q-laws dependent on the radial distance are adjusted (see Figure 3). A secant root finding algorithm has been applied for the calibration because the analytic derivative of any seismic field (see Eq. (5)) with respect to Q_p and Q_s implies a laborious work; see Gómez et al. (2020) for more details.

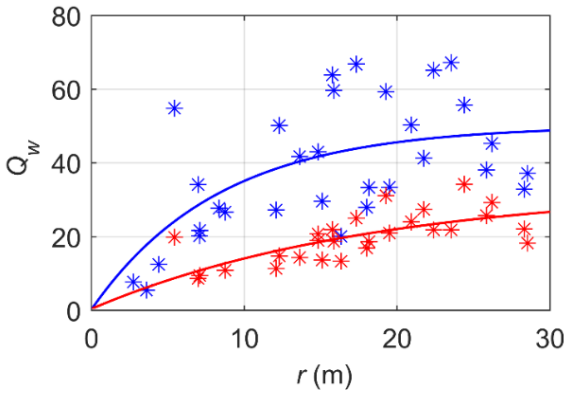

Figure 3. *Q*-laws for Q_p (blue) and Q_s (red).

Peak vibration levels from each blasthole have been predicted with Eq. (5) for the blasts under study considering data in Tables 1–4 and the *Q*-laws in Figure 3. The resulting values are plotted versus the scaled distance *SD*, i.e. ratio of distance to the gravity center of the blasthole divided by the square root of the explosive mass, as black triangles in Figure 4. The measured values are also plotted as reference (see colored markers). A linear fit of the peak measured values versus *SD* in log-log scale of the type $ppa = a_1 SD^{a2}$ has been made; the 95 % confidence bands (dashed magenta lines) of the regression and new predictions (dashed black lines) are also plotted. Figure 4 shows that the FFS values are fairly close to the fit line for measured values and in most cases within the regression confidence bounds.

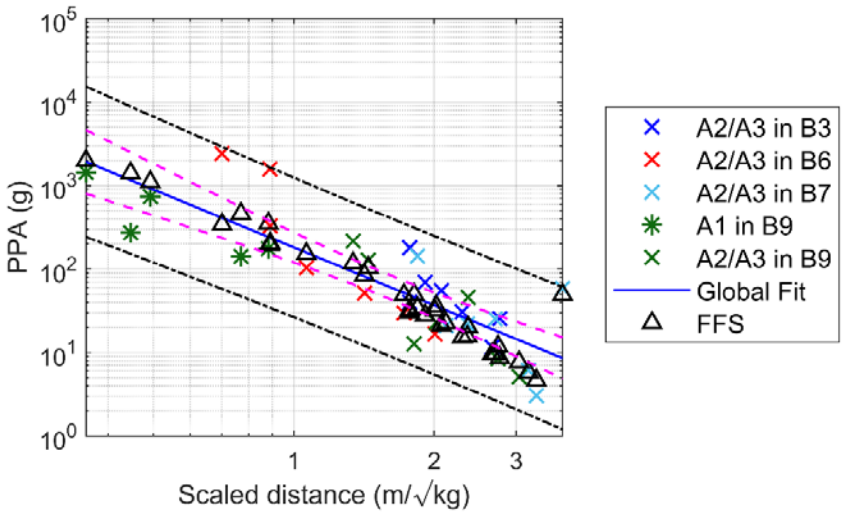

Figure 4. Measured and predicted peak accelerations versus scaled distance.

Sample application

A generic 44.5 mm (1¾ in) radius,10 m long blasthole composed of 11235 elements with a length of one hundredth of its radius is considered. The maximum radial distance is set in 6 m (19.7 ft). The mesh extends 5 m above the top and 1 m below the bottom of the blasthole, giving a domain of 16 × 6 m (52.5 × 19.7 ft). A 10 cm (3.94 in) square computational mesh was used, with a total of 9821 calculation points. Explosive parameters chosen are the mean of all available values obtained in the tests and are given in

Table 4. Rock properties are those in Table 1. Computation time varies between 0.5 s and 2 s per node and field depending on the length of the signal considered and the field evaluated, on a 2.2 GHz laptop. The resulting velocity radiation pattern of this simulation is shown as a contour plot in Figure 5 (left graph).

In order to provide a best-case scenario for the comparison of the H-P and the NIOSH-modified approaches with the FFS, the site specific constants in Eqs. 1 and 3 are estimated through a linear fit in log-log scale using the peak velocities calculated by the FFS itself, for the sample calculation. The main statistics of the fits are shown in Table 5 where the constants should be used with ppv (mm/s), distance (m) and charge (kg). In all cases, coefficients obtained are significant at a 0.05 level. The resulting velocity radiation patterns from the H-P and NIOSH modified models are also shown in Figure 5 (second and third graphs from the left, respectively). To facilitate the comparison between models, the ratio of the *ppv* from either H-P and NIOSH-modified approaches to the *ppv* from the FFS is calculated. Figure 5 shows the filled contour maps of ppv_{HP}/ppv_{FFS}, i.e. ratio between *ppv* from the H-P models and the FFS (fourth and fifth graphs from the left).

Table 5. Constants for H-P and NIOSH attenuation functions.

Approach	α	K	MAPLE[1]
H-P	0.752	218.613	23.68
NIOSH-modified	1.203	187.521	23.77

[1]Mean Absolute Percentage Logarithmic Error, see (Gómez et al., 2020).

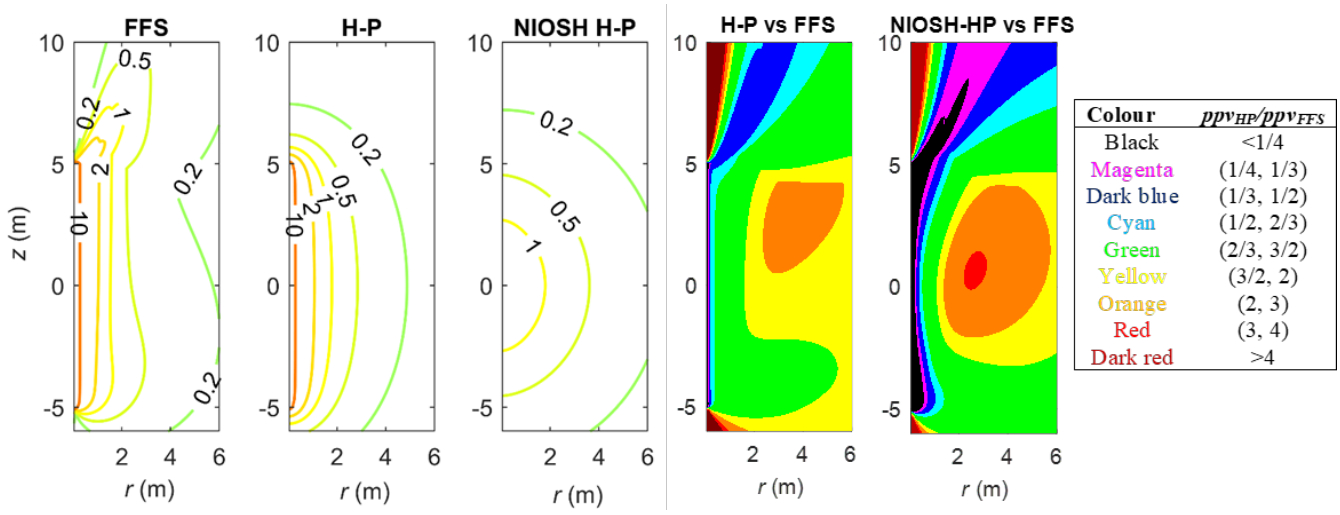

Figure 5. Contour maps of peak velocities from the FFS, the H-P model and NIOSH-modified approach (isolines of ppv are labelled in m/s, 32.8 6.6, 3.3, 1.6 and 0.7 ft/s), and filled countour maps of ratios betwen the H-P and NIOSH-modified models with respect to FFS.

Both H-P approaches underestimate—severely in the NIOSH-modified case—vibration levels with respect to the FFS in the upper zone offset from the hole. This is because the H-P calculations cannot predict the dominant component upwards, as the detonation is considered instantaneous. Conversely, both models overestimate peak velocities in the top and bottom zones of the rock, in the hole axis. The NIOSH-modified approach severely underestimates vibrations in the vicinity of the blasthole; this model uses an

average travel distance to the observation position that, close to the blasthole, is much longer than the actual distance, hence the *ppv* prediction there is very low. The H-P model does not show this malfunction (except in a very thin section adjacent to the hole), as the vibration components from the charge elements close to the observation point are calculated at their actual distances. There is a fair zone with similar patterns for both models, coaxial with the charge up to 1 to 2 m (3.28 to 6.56 ft) radial distance, widening upwards and downwards (see green patch). Further from the fair zone, both models overestimate vibrations in a kind of 'error islets' where errors increase to nearly 3-fold for the H-P model and 4-fold for the NIOSH-modified (see yellow, orange and red islets).

The FFS allows calculating the stress field, from which a damage pattern can be obtained. Two failure criteria based on *UCS*, *TS* and principal stresses produced by the radiated vibration, have been used to predict the extension of fracture zones. These are the maximum stress criterion and the Drucker-Prager yield criterion (Drucker & Prager, 1952) (Christensen, 2007). The latter has been chosen because the model considers an isotropic medium. The maximum stress criterion assumes that a material fails when the maximum principal stress (σ_1) in a material element exceeds *TS*. Alternatively, the material also fails if the minimum principal stress (σ_3) is less than *UCS*. Then the "safe" region for the material is assumed to be:

$$-UCS < \sigma_3 < \sigma_1 < TS \qquad \textbf{Equation 6}$$

The Drucker-Prager yield criterion leads to a "safe" region for the material defined by:

$$\left(\frac{1}{TS} - \frac{1}{UCS}\right)(\sigma_1 + \sigma_2 + \sigma_3) + \frac{1}{2 \cdot TS \cdot UCS}[(\sigma_1 - \sigma_2)^2 + (\sigma_2 - \sigma_3)^2 + (\sigma_3 - \sigma_1)^2] < 1 \qquad \textbf{Equation 7}$$

For the H-P and NIOSH models the breakage zones are delimited by (Persson et al., 1993):

$$ppv = \sigma / \left(\rho_r V_p\right) \qquad \textbf{Equation 8}$$

Where σ is a stress level (MPa) and ρ_r is the rock density.

Figure 6 shows the breakage zones observed in the FFS model. The first one (Crush Zone, CZ; red contour) is where the absolute value of σ_3 exceeds *UCS*. In that zone the rock breaks under compression. CZ extends 0.36 m (1.18 ft) along the entire length of the hole. The second one (Tensile Crack Zone, TCZ; yellow contour) is where σ_1 exceeds *TS*. In that zone the rock breaks under tension. It extends a constant value of 1.13 m (3.71 ft) in the central part of the graph as the detonation progresses, and up to 2.03 m (6.66 ft) in the upper zone of the hole due to the interruption of the detonation. The third zone (Drucker-Prager Zone, DPZ; light blue contour) is where the Drucker-Prager yield criterion is exceeded. It extends to about 1.5 m (4.92 ft) in the central part of the hole to 2.5 m (8.2 ft) in the upper part. Beyond that there is no damage to the rock from the seismic wave (dark blue contour). and the. Breakage zones for the H-P model and NIOSH modified-case are also plotted in Figure 6 (central and right graphs). In the H-P model, the CZ and TCZ extend 0.19 m (0.62 ft) and 2 m (6.56 ft), respectively. For the NIOSH modified-case there is no CZ because vibration levels predicted with Eq. (8) do not reach the UCS bound. One can note that both H-P approaches overestimate the extension of the TCZ with respect FFS, especially in the NIOSH modified case. The CZ in the H-P approach is thinner than in the FFS, whereas it is nonexistent in the NIOSH modified.

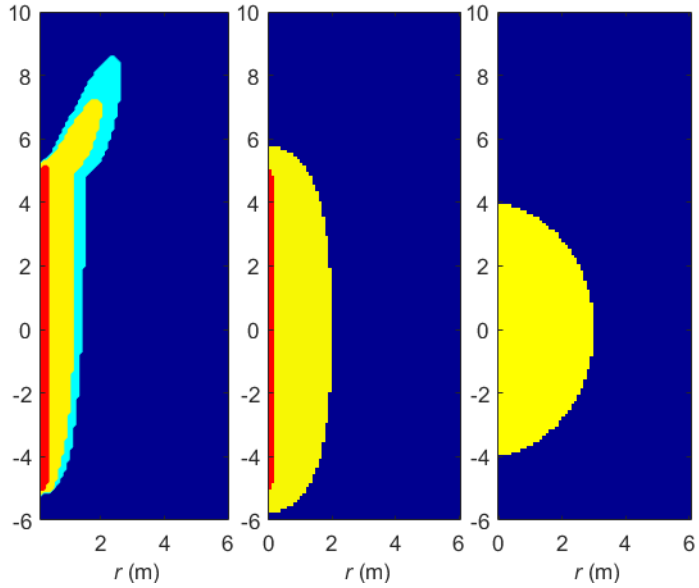

Figure 6. Damage zones from FFS (left), H-P model (center) and NIOSH-modified approach (right). CZ (red), TCZ (yellow), DPZ (light blue) and no damage (dark blue).

Conclusions

Vibration measurements from blasting tests have been used to develop a methodology to calibrate the FFS, noticeably the attenuation *Q*-factors, for which functions dependent of the distance to the blasthole have been established. The shock matching pressure of the detonation to the rock wall is used as peak pressure rather than the unrealistic von Neumann spike often used, a value not supported by physics since it belongs to the explosive unreacted hugoniot, and not to the shock hugoniot of rock.

The displacement field from the FFS is used to obtain the stress field, from which damage zones are obtained. Failure criteria based on *UCS, TS* and the principal stresses produced by the radiated vibration have been applied. The classical and widely used near-field Holmberg-Persson vibration model and its NIOSH modification have been compared with the full-field solution in terms of peak velocities (*ppv*) and damage zones. The main differences from the radiation patterns predicted by H-P and FFS are the absence of directionality of the *ppv* contours in the former. Contours are ellipsoidal for the H-P model and nearly spherical for the NIOSH modification, as no detonation drive upwards and no wave interferences take place. Values three times or one third the FFS values are common around the hole, even beyond those limits in some areas. The resulting damage zones from each model are significantly different. For the FFS, the damage penetrates 2.5 m (8.2 ft) away from the hole and three damage zones (crushed, tensile cracked and Drucker-Prager Zones) are identified moving radially away from the blasthole. The last one is not observed in both H-P approaches that predict a larger tensile cracked zone compared with the FFS. The crushed zone is not predicted by the NIOSH modification, while this is smaller for the H-P than for the FFS. These results together with the physical soundness of the FFS support its use over simpler, though physically questionable, models.

Acknowledgements

This work has been conducted under the SLIM project funded by the European Union's Horizon 2020 research and innovation program under grant agreement no. 730294.

References

Ahn, J. K., & Park, D. (2017). Prediction of Near-Field Wave Attenuation Due to a Spherical Blast Source. *Rock Mechanics and Rock Engineering*, *50*(11), 3085–3099. https://doi.org/10.1007/s00603-017-1274-3

Blair, D. P. (1990). Some problems associated with standard charge weight vibration scaling laws. *Int. Symp. on Rock Fragmentation by Blasting.*, 149–158. https://doi.org/10.1016/0148-9062(92)91889-d

Blair, D. P. (2003). A Fast and Efficient Solution for Wave Radiation from a Pressurised Blasthole. *Fragblast*, *7*(4), 205–230. https://doi.org/10.1076/frag.7.4.205.23533

Blair, D. P. (2007). A comparison of Heelan and exact solutions for seismic radiation from a short cylindrical charge. *Geophysics*, *72*(2), E33–E41. https://doi.org/10.1190/1.2424543

Blair, D. P. (2010). Seismic radiation from an explosive column. *Geophysics*, *75*(1), E55–E65. https://doi.org/10.1190/1.3294860

Blair, D. P. (2014). Blast vibration dependence on charge length, velocity of detonation and layered media. *International Journal of Rock Mechanics and Mining Sciences*, *65*, 29–39. https://doi.org/10.1016/j.ijrmms.2013.11.007

Blair, D. P. (2015a). The free surface influence on blast vibration. *International Journal of Rock Mechanics and Mining Sciences*, *77*, 182–191. https://doi.org/https://doi.org/10.1016/j.ijrmms.2015.04.006

Blair, D. P. (2015b). Wall control blasting. *11th International Symposium on Rock Fragmentation by Blasting*, 13–26.

Blair, D. P., & Minchinton, A. (1997). On the damage zone surrounding a single blasthole. *Fragblast*, *1*(1), 59–72. https://doi.org/10.1080/13855149709408390

Cho, S H, Miyake, H., Kimura, T., & Kaneko, K. (2003). Effect of the waveform of applied pressure on rock fracture process in one free-face model. *Science and Technology of Energetic Materials*, *64*(3), 116–125.

Cho, Sang Ho, & Kaneko, K. (2004). Rock Fragmentation Control in Blasting. *MATERIALS TRANSACTIONS*, *45*(5), 1722–1730. https://doi.org/10.2320/matertrans.45.1722

Christensen, R. M. (2007). A comprehensive theory of yielding and failure for isotropic materials. *Journal of Engineering Materials and Technology, Transactions of the ASME*, *129*(2), 173–181. https://doi.org/10.1115/1.2712847

Drucker, D. C., & Prager, W. (1952). Soil mechanics and plastic analysis or limit design. *Quarterly of Applied Mathematics*, *10*(2), 157–165.

Duvall, W. I. (1953). Strain-wave shapes in rock near explosions. *Geophysics*, *18*(2), 310–323. https://doi.org/10.1190/1.1437875

Gómez, S., Sanchidrián, J. A., & Segarra, P. (2020). Near-field vibration from blasting and rock damage prediction with a full-field solution. *International Journal of Rock Mechanics and Mining Sciences*, *134*. https://doi.org/10.1016/j.ijrmms.2020.104357

Gou, Y., Shi, X., Zhou, J., Qiu, X., Chen, X., & Huo, X. (2020). Attenuation assessment of blast-induced vibrations derived from an underground mine. *International Journal of Rock Mechanics and Mining Sciences*, *127*, 104220. https://doi.org/10.1016/j.ijrmms.2020.104220

Holmberg, R., & Persson, P.-A. (1978). *The Swedish approach to contour blasting*. SveDeFo.

Hustrulid, W., & Lu, W. (2003). The Lu-Hustrulid approach for calculating the peak particle velocity caused by blasting. *Explosives and Blasting Technique*, 291–300. https://doi.org/10.1201/9781439833476.ch36

Iverson, S., Kerkering, C., & Hustrulid, W. (2008). Application of the NIOSH-Modified Holmberg-Persson Approach to Perimeter Blast Design. *National Institute for Occupational Safety and Health*.

Kjartansson, E. (1979). Constant Q-wave propagation and attenuation. *Journal of Geophysical Research: Solid Earth*, *84*(B9), 4737–4748. https://doi.org/10.1029/JB084iB09p04737

Meredith, J. A. (1990). *Numerical and Analytical Modelling of Downhole Seismic Sources: The Near and Far Field. PhD Thesis. Massachussetts Institute of Technology*. Massachusetts Institute of Technology.

Meredith, J. A., Toksöz, M. N., & Cheng, C. H. (1993). Secondary shear waves from source boreholes. *Geophysical Prospecting*, *41*(3), 287–312. https://doi.org/10.1111/j.1365-2478.1993.tb00571.x

Meyers, M. A. (1994). *Dynamic behaviour of materials*. John Wiley & Sons, Inc.

Meza-Fajardo, K. C., & Lai, C. G. (2007). Explicit causal relations between material damping ratio and phase velocity from exact solutions of the dispersion equations of linear viscoelasticity. *Geophysical Journal International*, *171*(3), 1247–1257. https://doi.org/10.1111/j.1365-246X.2007.03590.x

Minchinton, A. (2015). On the Influence of Fundamental Detonics on Blasting Practice. *11th International Symposium on Rock Fragmentation by Blasting*, 41–54.

Persson, P.-A., Holmberg, R., & Lee, J. (1993). *Rock Blasting and Explosives Engineering*. CRC Press.

Ricker, N. (1953). The form and laws of propagation of seismic wavelets. *Geophysics*, *18*(1), 10–40. https://doi.org/10.1190/1.1437843

Rossmanith, H. P., & Kouzniak, N. (2004). Supersonic Detonation in Rock Mass - Part 2: Particle Displacements and Velocity Fields for Single and Multiple Non-Delayed and Delayed Detonating Blastholes. *Fragblast*, *8*(2), 95–117. https://doi.org/10.1080/13855140412331336179

Salum, A. H., & Murthy, V. M. S. R. (2019). Optimising blast pulls and controlling blast-induced excavation damage zone in tunnelling through varied rock classes. *Tunnelling and Underground Space Technology*, *85*, 307–318. https://doi.org/10.1016/j.tust.2018.11.029

Sharpe, J. A. (1942). The production of elastic waves by explosion pressures. I. Theory and empirical field observations. *Geophysics*, *7*(2), 144–154. https://doi.org/10.1190/1.1445002

Silva, J., Worsey, T., & Lusk, B. (2019). Practical assessment of rock damage due to blasting. *International Journal of Mining Science and Technology*, *29*(3), 379–385. https://doi.org/10.1016/j.ijmst.2018.11.003

Tubman, Keneth M. (1984). *Full Waveform Acoustic Logs in Radially Layered Boreholes. PhD Thesis. Massachussetts Institute of Technology*. Massachusetts Institute of Technology.

Tubman, Kenneth M, Cheng, C. H., & Toksöz, M. N. (1984). Synthetic full waveform acoustic logs in cased boreholes. *Geophysics*, *49*(7), 1051–1059. https://doi.org/10.1190/1.1441720

Uenishi, K., & Rossmanith, H. P. (1998). Blast wave propagation in rock mass—Part II: Layered media. *Fragblast*, *2*(1), 39–77. https://doi.org/10.1080/13855149809408879

Vanbrabant, F., Chacón, E. P., & Quiñones, L. A. (2002). P and S Mach Waves Generated by the Detonation of a Cylindrical Explosive Charge – Experiments and Simulations. *Fragblast*, *6*(1), 21–35. https://doi.org/10.1076/frag.6.1.21.8849

Zel'dovich, Y. B., & Raizer, Y. P. (2002). *Physics of Shock Waves and High-Temperature Hydrodynamic Phenomena*. Dover Publications.